Coastal Engineering 60 (2012) 248–260

Contents lists available at SciVerse ScienceDirect

Coastal Engineering

journal homepage: www.elsevier.com/locate/coastaleng

On the importance of high frequency tail in third generation wave models

S. Mostafa Siadatmousavi [a,b,*], F. Jose [b], G.W. Stone [a,b]

[a] Department of Oceanography and Coastal Sciences, Louisiana State University, Baton Rouge, LA 70803, USA
[b] Coastal Studies Institute, Louisiana State University, Baton Rouge, LA 70803, USA

ARTICLE INFO

Article history:
Received 19 January 2011
Received in revised form 25 September 2011
Accepted 31 October 2011
Available online 30 November 2011

Keywords:
Wave spectrum
White capping
SWAN
WAVEWATCH-III
High frequency tail
Gulf of Mexico

ABSTRACT

Two well-known third generation wave models, SWAN and WAVEWATCH-III, with different assumptions for high cut-off frequency were used to evaluate the interaction of low and high frequency components in wave spectral evolution. The results showed that WAM cycle 3 formulation overestimates the energy content in frequency band of 0.5–1 Hz for Gulf of Mexico, which suggests using cut-off frequency close to 0.5 Hz rather than 1 Hz would improve the simulated bulk wave parameters. The evaluation of WAM cycle 4 and a newer nonlinear formulation implemented recently for white capping in SWAN also showed the better performance of wave model in oceanic scale with cut-off frequency close to 0.5 Hz. However, WAM cycle 3 was more sensitive to cut-off frequency as well as to the exponent used in the expression for the frequency tail, than other formulations in SWAN. The use of f^{-5}tail shape, rather than the f^{-4} form for the frequency spectrum beyond both cut-off frequencies used in this study, resulted in better agreement between simulated and observed wave parameters for most of the formulations implemented in these models. Also, it was demonstrated that WAM cycle 3 with dynamic cut-off frequency outperformed the corresponding configuration with static cut-off frequency. The suggested modifications for cut-off frequency and the expression for high frequency tail in SWAN substantially ameliorates the widely known underestimation of the average wave period associated with the WAM cycle 3 formulation, and reduces the amount of calculations needed for other formulations.

Published by Elsevier B.V.

1. Introduction

Third generation phase-averaged wave models are efficient tools for simulating wave field in medium- and large-scale domains (Zubier et al., 2003). These models are based on the wave action balance equation, and is given by

$$\frac{DN}{Dt} = \frac{S}{\sigma} \tag{1}$$

in which $N \equiv F/\sigma$ is wave action density, F is wave energy density, $\sigma = 2\pi f$, in which f denotes relative frequency, and S is the total of source/sink terms. Wind input, quadruplet wave–wave interaction and energy dissipation are the most common source/sink terms in deep water wave equation (Komen et al., 1994). Several packages have been suggested for energy transfer from wind to waves and wave energy dissipation, to be implemented in third generation wave models (Babanin et al., 2010; Cavaleri et al., 2007; Komen et al., 1984; Rogers et al., 2003; Tolman and Chalikov, 1996; van der Westhuysen et al., 2007); including WAM cycle 3 (WAM-3 here after) and WAM cycle 4 (WAM-4 here after) formulations. In his pioneering work, Komen et al. (1984) showed that pulse-based quasi-linear model of Hasselmann (1974) proposed for calculating the white capping term, and rescaled wind input formulation of Snyder et al. (1981), were able to reproduce the fully developed wind sea. These formulations became the core of the WAM-3 wave model. A more detailed understanding of the complex interaction of wind and waves in energy transfer to waves resulted in a newer wind input formulation (Janssen, 1991) and was incorporated in WAM-4; along with dissipation term with quadratic dependence on the wave number, to provide more dissipation in high frequency end of the spectrum (Janssen, 2004). The dependence of wave dissipation on mean wavenumber and steepness in WAM formulation resulted in erroneous over-prediction of wind sea in the presence of swell waves (van der Westhuysen et al., 2007). The field evidence do not confirm the enhanced growth of wind sea in combined sea-swell environment (Ardhuin et al., 2007; Young and Babanin, 2006). To solve this problem, van der Westhuysen et al. (2007) suggested a nonlinear saturated-based white capping equation which was entirely local in the frequency domain (Westhuysen hereafter). Their package also included the wind energy transfer of Yan (1987) which was in better agreement with observations than Snyder et al. (1981) during strongly forced waves. Tolman and Chalikov (1996) suggested two different mechanisms for dissipation of energy in high and low ends of the spectrum. In their source package (TC hereafter) the low frequency

* Corresponding author at: Department of Oceanography and Coastal Sciences, Louisiana State University, Baton Rouge, LA 70803, USA. Tel.: +1 225 578 4728; fax: +1 225 578 2520.
E-mail address: ssiada1@lsu.edu (S.M. Siadatmousavi).

0378-3839/$ – see front matter. Published by Elsevier B.V.
doi:10.1016/j.coastaleng.2011.10.007

dissipation term was based on the analogy with turbulence, while an empirical formulation was used for the high frequency constituents. The energy transfer formulation of Chalikov (1995) and Chalikov and Belevich (1993) was employed in TC, which takes into account energy transfer from waves to wind when the waves move faster than wind or travel at a larger angle with wind direction.

Although an exact expression for calculating nonlinear quadruplet wave–wave interaction is formulated, to use in third generation wave models (van Vledder, 2006), it is not feasible to implement it for operational wave forecasting purposes, due to intense numerical calculations involved. By considering only a few configurations from all plausible combinations of interacting wavenumbers, Discrete Interaction Approximation (DIA) provides a fast estimation of wave–wave interaction term in third generation operational wave models (Hasselmann et al., 1985). Although this method is criticized to be oversimplified to produce an exact wave spectrum (Hasselmann and Hasselmann, 1985; van Vledder, 2006; van Vledder and Bottema, 2003), it has proved itself to be accurate enough to reproduce bulk wave parameters (Janssen et al., 1994).

As its name implies, nonlinear wave interaction is not at all local in the frequency domain; i.e., computation of nonlinear energy transfer for a specific frequency component f_i, requires information about energy content at frequencies higher and lower than f_i. However, in order to numerically compute the nonlinear term, a third generation model needs to compute source/sink terms on a limited number of frequency components. To calculate the energy transfer due to quadruplet wave–wave interaction at f_i, DIA requires energy level at $0.75f_i$ and $1.25f_i$. Since the forward face of a typical spectrum is steep, the assumption of zero energy for frequencies lower than the first frequency component (f_1), is justifiable if f_1 is selected small enough. The recommended value for $f_1$is 0.03–0.04 Hz (Janssen, 2008). However, wave energy decays slowly at the rear face of the spectrum. Therefore, beyond the highest frequency considered in the prognostic region of the wave spectrum, f_H, a diagnostic frequency tail is added in third generation wave models. This high frequency tail is used to calculate bulk wave parameters as well as the quadruplet wave–wave interaction (Hasselmann, 1988), and has the following general form:

$$F(f,\theta) = F(f_H,\theta)\left(\frac{f}{f_H}\right)^{-n} \quad for f > f_H \tag{2}$$

in which θ denotes wave direction, and n is a constant . The main objective of this study is to evaluate the sensitivity of advanced wave models to n and f_H, and thereby to provide a good estimation of n, based on skill assessment of the model against data from an array of NDBC buoys in the Gulf of Mexico; which in turn would help in eventual optimization of oceanic scale application of well-known third generation wave models.

Also, it has to be reminded that in shallow waters, the S term in Eq. (1) includes more terms/processes. Wave dissipation due to bottom friction becomes important in shallow water, especially during high energy events (Li and Mao, 1992). The substantial damping of waves due to complex interaction with cohesive sediment bottom also has to be considered for deltaic coasts (Sheremet and Stone, 2003). The rate of energy dissipation is roughly estimated as a few watts per square meter, approximately the same as the rate of energy transferred from wind to the sea surface during moderate wind conditions (Cavaleri et al., 2007). However, considering the depth of NDBC buoys used in this study, the shallow water processes has insignificant influence on the results.

1.1. Previous studies on high frequency range of the wave spectrum

Several theoretical and experimental studies have been carried out over the last few decades to describe the high frequency end of the spectrum. Phillips (1958) envisaged a saturation upper limit on the spectral level, independent of the strength of forcing wind. In this theory, when the local downward acceleration exceeds g, the wave breaks and transfers its energy to turbulence. Based on similarity arguments, it resulted in k^{-3}power law for a one dimensional wavenumber spectrum, and f^{-5} power law for frequency spectrum. Mitsuyasu (1977) found this theory valid for $0.6<f<4$ Hz, while the wind speed $U_{10.5}$ was 8 m/s and fetch was 2 km. However, he found f^{-4} relation for $4<f<15$ Hz. Kitaigordskii et al. (1975) suggested the incorporation of water depth, h, to Phillips' (1958) theory to make it applicable in shallow water also. Using a similar method, they suggested hf^{-3}would work well for a shallow basin with a mean depth of 4 m. Based on the similarity argument on wave speed, c, instead of acceleration, Thornton (1977) suggested the high frequency tail form of c^2f^{-3}, which can be simplified to f^{-5} power law in deep water and hf^{-3}in shallow water.

Toba (1973) argued that the equilibrium range of spectrum above peak frequency must also depend on wind friction velocity, u^*, and proposed the form of u^*f^{-4}. Anctil et al. (1993) observed f^{-4}relation on high frequency band of a NDBC buoy with a 0.5 Hz cut-off frequency. Several other datasets are also available in favor of the f^{-4}relation (Donelan et al., 1985; Kahma, 1981).

Based on the existence of the Kolmogoroff-type equilibrium range for water waves, Kitaigorodskii (1983) proposed a theoretical explanation for the f^{-4}tail form. The direct measurements of energy input from wind to waves showed that energy transfer to waves was not concentrated at wavenumbers close to the spectral peak (Snyder et al., 1981), which was in direct contradiction with the assumptions of Kitaigorodskii (1983). The most comprehensive theory in support of the f^{-4}shape was proposed by Phillips (1985) which assumed that deep water source and sink terms were important in the equilibrium range of the spectrum. Also, note that the nonlinear interaction plays an important role in the existence of an ordered high frequency tail, and tends to maintain an f^{-4}tail form in the absence of other source terms at frequencies higher than $1.5f_p$ (Resio and Perrie, 1991), in which $f_p$was the peak frequency.

However, there are some recent studies which are in general agreement with the f^{-5} power law (Banner et al., 1989; Hwang et al., 1996). The high variability in the slope of spectrum at high frequency range was observed in different datasets. Leykin and Rozenberg (1984) measured the frequency spectra from the Caspian Sea up to 10 Hz, and found that the frequency range of 2.4–7.2 Hz follows the power law model with the exponent varying between -3.2 and -4.8. They also claimed a fair agreement with the f^{-4}relation for $1.2<f/f_p<3.2$ Hz. Based on recorded wave data from the Great Lakes, Liu (1989) reported that the exponent varied from -3 to -5. He suggested the f^{-4}relation for growing young wind seas and the f^{-3}relation for fully developed spectra. The data from a series of wave gauges established in Lake George, Australia, also suggested the use of variable exponents when discussing the spectral evolution (Young and Verhagen, 1996).

Different explanations were suggested for the uncertainty in the high frequency tail of the wave spectrum. Rodriguez and Soares (1999) attributed this to intrinsically random variability of wind-generated waves. Another group of studies relates the variability of the exponent to the range of frequencies used to determine the power law model. Those studies suggested that close to spectral peak, a f^{-4}power law holds while at frequencies higher than $(2.5-3.5)f_p$, the tail maintains a f^{-5}form (Ewans and Kibblewhite, 1990; Forristall, 1981; Hansen et al., 1990; Mitsuyasu et al., 1980; Rodriguez et al., 1999). Banner (1990, 1991), assumed a k^{-4}tail form for two dimensional wavenumber spectrum (corresponding to k^{-3}tail form for an omni-directional wavenumber spectrum), and showed that the change in slope of frequency spectrum could be explained by frequency dependence of the directional spread of energy. He also showed that the Doppler shifting effect caused by orbital

velocity of dominant wave component becomes important for $f/f_p > 3$ and may modify the f^{-5} tail shape.

2. Third generation wave models and high frequency tail

The cut-off frequency is determined either statically or dynamically in different third generation wave models. The idea behind dynamic cut-off frequency is to save the computational resources by skipping the calculations for frequencies which are far from the peak frequency. In this study, one model from each of these two types was selected, and different source packages were employed in each model to ensure insensitivity of the conclusions to a particular model or formulation.

2.1. SWAN

SWAN (Simulating WAves Nearshore) is a well-documented wave model, developed originally to simulate shallow water wave transformation, by Delft University of Technology (SWAN team, 2010). Unlike most popular third generation wave models, SWAN employs implicit scheme to solve Eq. (1) in the (σ, θ) spectral domain. Therefore, time step is mainly determined by the desired temporal accuracy, rather than the restriction by stability criteria of an explicit scheme in shallow water. Since version 40.72, SWAN provides an opportunity to use the Finite Volume method to solve the wave action conservation equation on an unstructured triangular mesh; so that the user can incorporate a finer mesh for zones of interest, with approximately no change in total computational cost, and still use coarser grids where sharp modification in energy spectra is not expected.

In this study, SWAN (version 40.72) was used with default coefficients for WAM-3, WAM-4 and Westhuysen formulations for transfer of wind energy to waves, and for the white capping in different meteorological conditions. The nonlinear quadruplet wave–wave interaction was considered with DIA method; linear wave growth according to Cavaleri and Rizzoli (1981); depth-induced wave breaking according to Battjes and Janssen (1978) and bed friction according to the JONSWAP formulation (Hasselmann et al., 1973).

SWAN uses static cut-off frequency, and the highest frequency, f_H, in Eq. (2) could be set by the user as a constant number (1 Hz and 0.515 Hz were compared in this study). The exponent n in Eq. (2) is set to $n=4$ for WAM-3 and Westhuysen formulations while $n=5$ is set for WAM-4 formulation.

2.2. WAVEWATCH-III

WAVEWATCH-III is developed at the Marine Modeling and Analysis Branch of National Centers for Environmental Prediction, NOAA. It was designed originally for deep water wave evolution and transformation, and considered to be very efficient at oceanic scales. However, since its latest version, 3.14, it also includes formulations for most of the shallow water processes. WAVEWATCH-III employs either explicit third order scheme called ULTIMATE QUICKEST or the explicit first order upwind scheme to solve the wave action balance equation in the spectral domain (k, θ) (Tolman, 2009). Similar equations to SWAN were used in WAVEWATCH-III, for the nonlinear quadruplet wave–wave interaction, linear wave growth, depth-induced wave breaking and bed friction process.

The highest frequency f_H in WAVEWATCH-III follows the original WAM dynamic cut-off frequency, and set as maximum of a) 2.5 times the mean frequency of current wave spectra, b) 4 times of the mean frequency of the Pierson and Moskowitz (1964) frequency. The first limit was used for young seas, and equilibrium range was expressed in terms of mean frequency instead of peak frequency because it was numerically more stable. The second limit was designed for fully developed conditions. Moreover the calculated value for f_H cannot exceed the user defined value (0.515 Hz was used in this study). According to Tolman (1992), the dynamical integration scheme used in WAVEWATCH-III results in a smoother high frequency tail, if $n=4.5$ is used for the WAM-3 formulation. However, $n=5$ is the default value for the TC formulation.

Moreover, the code of WAVEWATCH-III-3 formulation was modified to use WAM-3 with static cut-off frequency, to compare the performance of a model using dynamic and static cut-off frequencies.

2.3. Interaction of frequency tail and energy evolution in wave models

In their pioneering study, Komen et al. (1984) showed the success of third generation wave models in reproducing the saturation spectrum. However they assumed a power law for the high wavenumber end of the spectrum to reduce the computational needs. Use of a different tail power showed insensitivity of the model performance to the value of n used in Eq. (2) (Komen et al., 1994). This was in agreement with studies that demonstrated a weak coupling between the tail of the spectrum and spectral peak (Hasselmann, 1963; Young and Vanvledder, 1993); however, the detailed analysis by Banner and Young (1994) bolstered the importance of frequency tail in the evolution of wave spectrum. That particular study showed that, as a result of nonlinear wave–wave interaction, the model with an unconstrained tail (with a corresponding large f_H, so that the model would calculate the energy content at frequencies a few times above of the peak frequency) had much more energy in the high frequency end of the spectrum, and hence slower growth close to the spectral peak. Their modeling results demonstrated that variants of WAM dissipation terms could not reproduce reasonable energy in the frequency tail and directional spread simultaneously. The study also concluded that a reasonable estimation from wave model was critically dependent on establishing an artificial diagnostic tail.

3. Simulations

3.1. Model setup

In order to investigate the degree to which the high frequency tail of the spectrum can affect the computation of bulk wave parameters, a parallel implementation of unstructured SWAN (ver 40.72) and WAVEWATCH-III (ver 3.14) was used to simulate the waves in the Gulf of Mexico. The BatTri package (Bilgili et al., 2006) was used to generate the mesh file for SWAN, considering all quality criteria explained in the SWAN Manual (SWAN team, 2010); such as to avoid a steep element slope, very small vertex angles, or significant change in mesh size relative to the adjoining mesh elements. The mesh was partitioned into 70 sub-grids with approximately the same number of nodes in each partition, using *adcprep*, the grid preparation module for the circulation model ADCIRC (Westerink et al., 1992). The mesh file and its sub-grids are shown in Fig. 1 which consist of 32,235 nodes and 59,258 triangles, with the element length varying from 1 km nearshore to 50 km in deeper water. A structured grid with spatial resolution of 0.1° (~10 km) was used in WAVEWATCH-III. In both models, directional resolution was set at 10°, and frequency exponential was 1.1 and the lowest frequency was set to 0.035 Hz. The highest frequency close to 0.5 Hz is a typical choice for present-day wave forecasting systems (Janssen, 2008) therefore 0.515 Hz is used as highest cut-off frequency in WAVEWATCH-III. However, for SWAN, it is suggested to use 1 Hz as the cut-off frequency (SWAN team, 2010). Therefore two sets of simulations were performed with SWAN, using the two high cut-off frequencies, viz., 0.515 and 1 Hz.

Two simulation periods, corresponding to two contrasting high energy met-ocean conditions, were considered in this study to evaluate the performance of wave models with different assumptions for the high frequency end of the spectrum. The first period, 0000 UTC on 22 August 2008 to 2100 UTC on 16 September 2008, includes

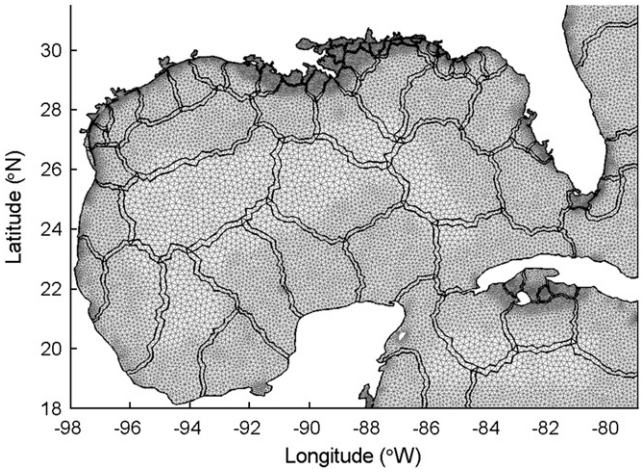

Fig. 1. The computational mesh for the Gulf of Mexico domain and its partitions for parallel computing using 70 processors. The data communications between the neighboring sub-grids were effected through the common vertices along the boundaries, which are highlighted with dark curves.

hurricane Gustav and hurricane Ike, as well as a period of fair weather conditions in between. The tracks of these hurricanes as well as the locations of *in situ* observations are shown in Fig. 2. To prepare the wind field, the velocity components were extracted from the North American Regional Re-analyzed (NARR) database from the National Center for Environmental Prediction (NCEP/NOAA) server. The data were combined with high resolution H* wind data obtained from the Atlantic Oceanographic and Meteorological Laboratory (AOML/NOAA) database to have better spatial and temporal resolution as well as for avoiding underestimation during storms (Swail and Cox, 2000). More details on hurricanes Gustav and Ike, and preprocessing of wind data used for wave simulation are presented elsewhere (Berg, 2008; Beven and Kimberlain, 2008; Siadatmousavi et al., 2009). Another longer simulation period, from 0000 UTC on 20 October 2007 to 0000 UTC on 1 May 2008, was also considered to evaluate the performance of models during the passage of extra-tropical winter storms (Cold Fronts) as well as for the intermittent fair weather (calm). Since the models were initiated with *cold start* conditions, no output from the first two days for the first simulation, and the first 10 days for the second simulation, was used in skill assessments of the models.

3.2. Skill assessment of SWAN

Significant wave height (H_s), peak period (T_p) and average period (T_a) computed for the first time period (hurricane conditions) were compared with data from NDBC 42040 in Fig. 3. In this case, WAM-3 formulation of SWAN with $f_H = 1$ Hz and $n = 4$ and $n = 5$ as tail exponents, was used. Note that T_{m02} (square root of the ratio between zero- and second-moment of frequency spectrum) was used to estimate T_a, from the wave spectrum. To be consistent with *in situ* observations, all bulk wave parameters were estimated based on the wave spectrum up to 0.485 Hz. The wind speed used for simulation and the measured wind speed at the buoy location (NDBC 42040) are provided in panel (a), for reference. As shown in panel (b), when $H_s < 1$, the simulated H_s was significantly affected by the exponential term in Eq. (2). In this lower range of H_s, WAM-3 performs better with $n = 5$ rather than $n = 4$. Panel (c) shows the same improvement in terms of T_p prediction using $n = 5$ in fair weather conditions. Panel (d) confirms that T_a shows a systematic increase when using $n = 5$, rather than the default value $n = 4$.

In Fig. 4 spectral evolutions are compared for the two frequency tail configurations against in *situ* measurements from NDBC buoy 42040. It is clear that spectra simulated by both model configurations are too wide compared with the buoy measurements; however, $n = 5$ leads to more realistic and narrower distribution of energy; especially the energy levels at the high frequency end of the spectra are lower for $n = 5$. As shown with more extended contour lines over the frequency band of 0.15–0.25 Hz, the wave energy is dissipated with slower pace for $n = 5$ than $n = 4$, which is in accordance with buoy data shown in panel (c).

Changing the exponent n from 4 to 5 resulted in the same effects on the bulk wave parameters and wave spectrum at all stations shown in Fig. 2, when using the WAM-3 formulation. In order to demonstrate the effects of the change in high frequency shape on the model's performance at all measurement locations, it is ideal to use some statistical parameters. Although the Scatter Index (SI), root mean square error (RMSE), correlation coefficient (R^2) and bias are

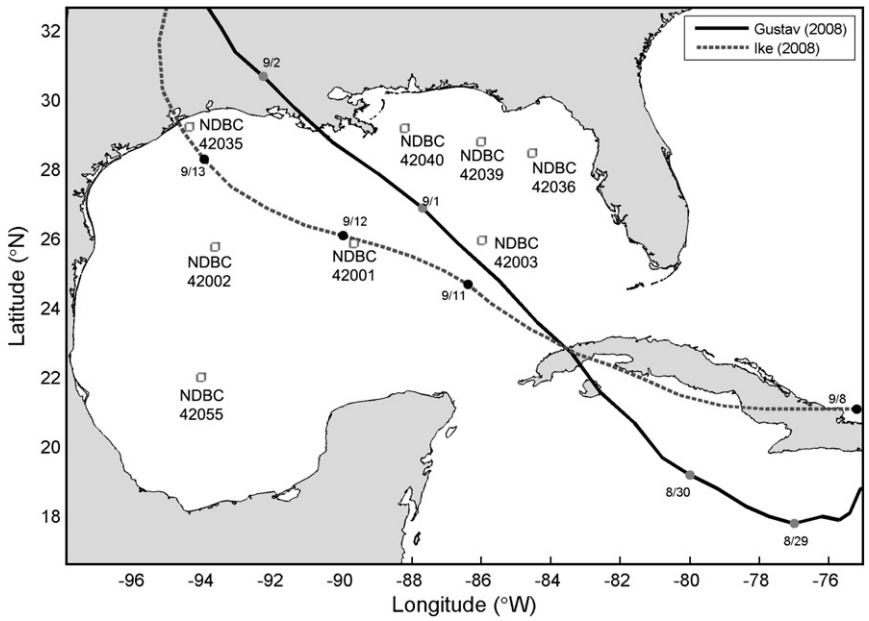

Fig. 2. The track of hurricanes Gustav and Ike in Gulf of Mexico and the Caribbean Sea. (Data courtesy: National Hurricane Center). The locations of NDBC Buoys used in this study are also provided.

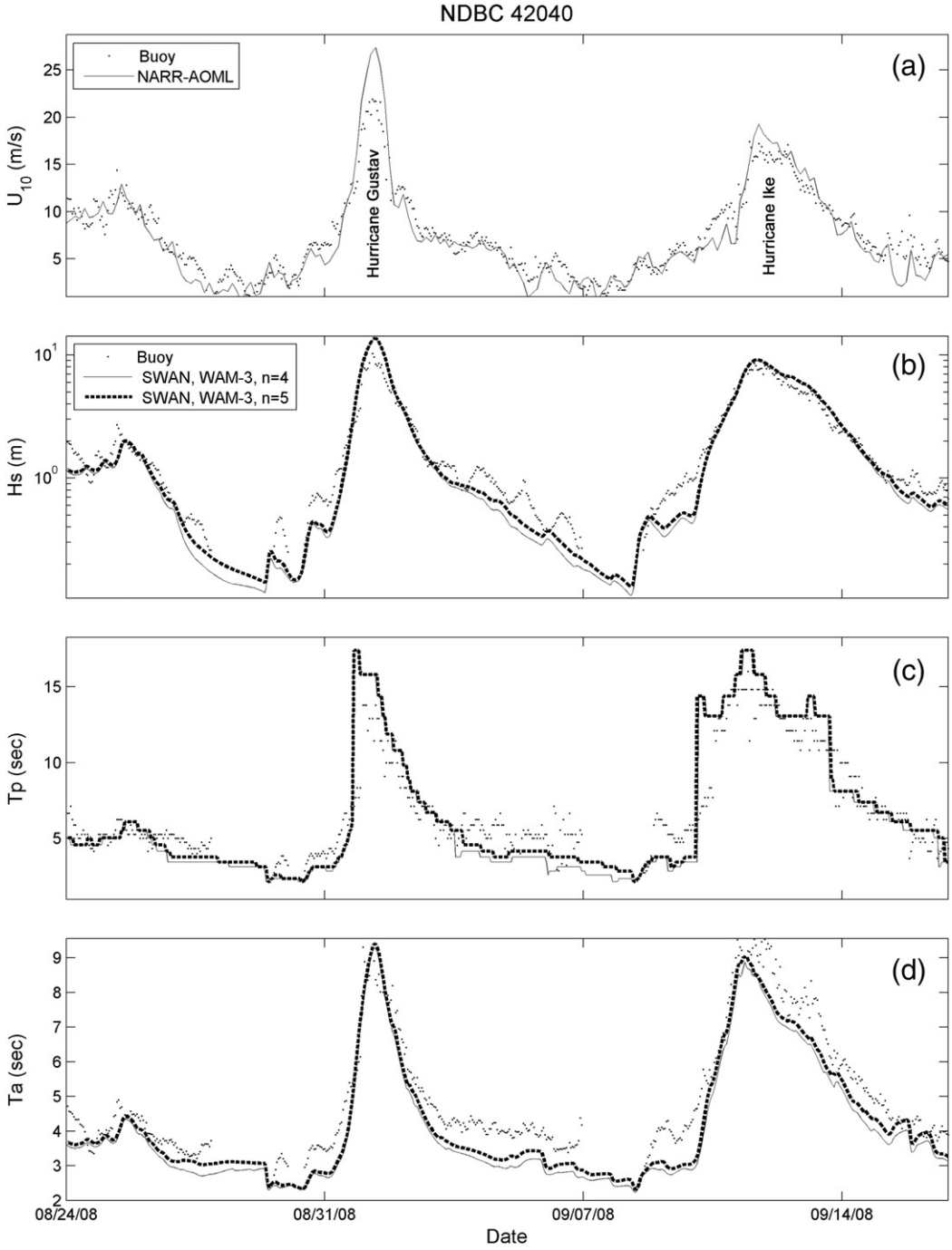

Fig. 3. Skill assessment of WAM-3 formulation of SWAN using $n=4$ and $n=5$, in terms of bulk wave parameter; using *in situ* data from NDBC 42040: a) time series of wind speed at 10 meter above sea level plotted against a high resolution blended wind (AOML H* wind and NARR/NCEP); (b) Significant wave height; (c) Peak wave period; (d) Average wave period. Note that logarithmic scale is used for wave height, to show the performance of wave model in both severe and calm weather conditions.

the most common statistical parameters used to evaluate the performance of wave models over the years (Alves et al., 2002; Ardhuin et al., 2010; Janssen, 2008), these parameters are best for the description of average behavior of models over an extended period of time; or for a dataset with some sort of similarities. The first simulation period encompasses both fair weather and two severe hurricane conditions; while the overall performance of the wave model, covering both energetic and calm weather conditions, was the main interest of this study. In addition, it is better to avoid separation of these two conditions, because it would make the outcome of the analysis subjective to the criteria used for such a separation. Therefore a normalized RMSE (NRMSE) is used to measure the overall performance of the wave model in both calm and severe weather conditions. The following definition is used for NRMSE in this study:

$$\mathrm{NRMSE} = 100 \times \sqrt{\frac{1}{N}\sum_{i=1}^{N}\left(\frac{X_{Oi}-X_{Mi}}{X_{Oi}}\right)^2} \tag{3}$$

In which X_{Oi} and X_{Mi} denote ith data resulted from observation and model respectively, and N is the total number of data points. Note that the data with the observed H_s below 0.3 m was removed before calculating the statistical parameters, to avoid any sensitivity to division by small numbers, as well as low signal-to-noise ratio for

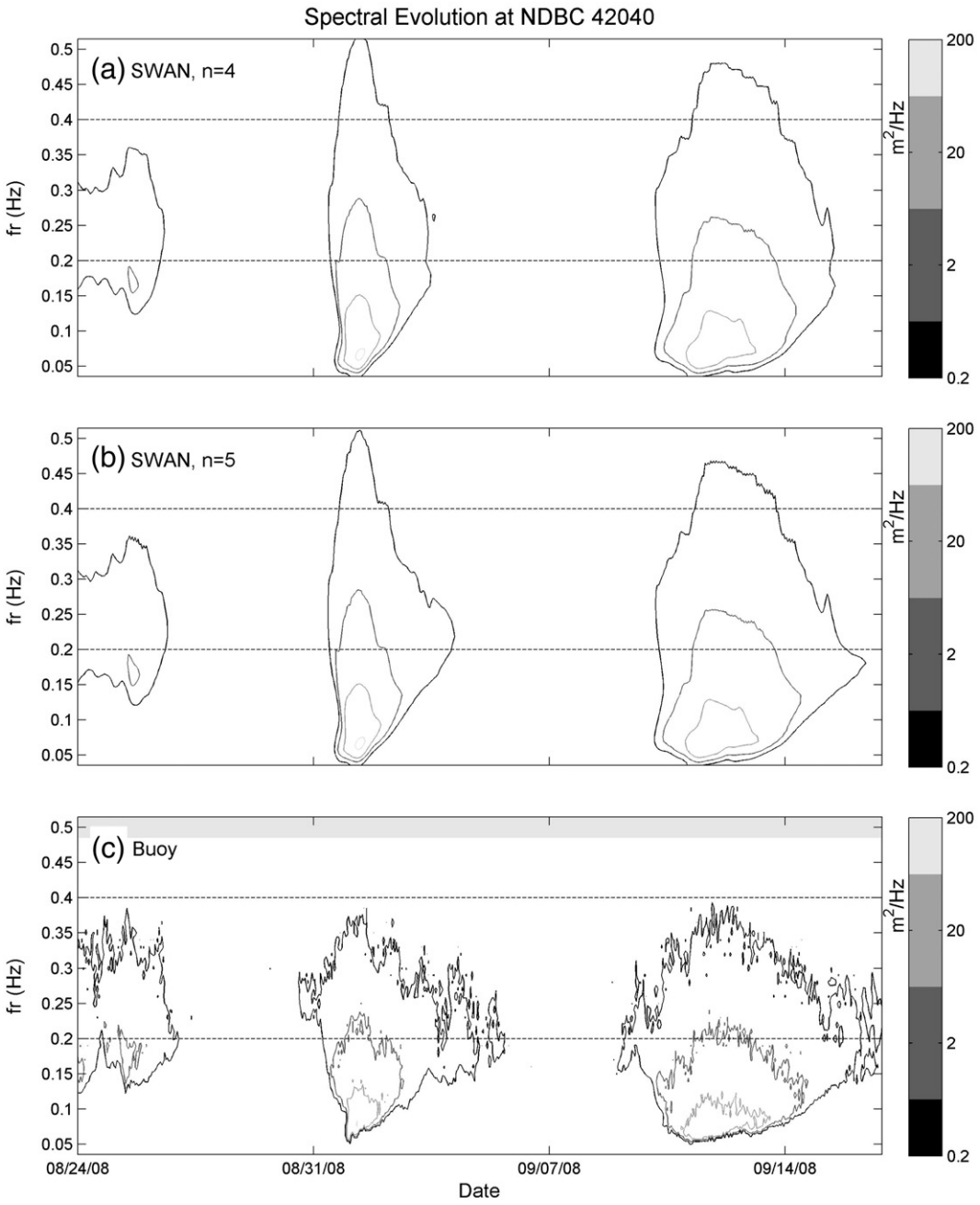

Fig. 4. The spectral evolution computed at NDBC buoy 42040 for the first time period (2008 Hurricane conditions) for a) SWAN with WAM-3 formulation and exponent of $n=5$ in tail formula; b) SWAN with WAM-3 formulation and exponent of $n=4$ in tail formula; c) spectra measured by the buoy. The maximum frequency reported at buoy 42040 was 0.485 Hz. The dash lines at 0.2 Hz and 0.4 Hz were also plotted for reference. Note that the contours are in logarithmic scales.

the data measured at such a calm weather condition. Another useful statistical parameter is the bias, which is defined as:

$$\text{Bias} = \sum_{i=1}^{N} (X_{Mi} - X_{Oi}) \tag{4}$$

For all NDBC stations shown in Fig. 2, which did not fail during the passage of hurricanes Gustav and Ike in 2008, the statistical parameters were computed from SWAN simulations, using the WAM-3 formulation with $n=4$ and $n=5$, and presented in Fig. 5. The bulk wave parameters were calculated based on instrument cut-off frequency which was at 0.485 Hz for buoys. Using $n=5$, instead of $n=4$, could systematically decrease the NRMSE and bias of T_a at all stations. It also lowered the NRMSE of T_p and H_s due to better predictions during fair weather conditions. The use of $n=4$ resulted in negative bias (under estimation) of T_p in all stations but $n=5$ partially fixed the underestimation of T_p. Note that the H_s bias was not markedly affected by the change in the power of high frequency tail; and in terms of NRMSE, in all stations, $n=5$ resulted in better agreement with *in situ* measurements.

The mean value of Bias and NRMSE for the result of SWAN using different formulation at all stations are presented at Fig. 6. It illustrates that the interaction of the high frequency end of the spectrum and the performance of the wave model depends not only on the formulations used for wave dissipation and energy tranfser from wind to waves, but also on the assumptions for high frequency cut-off used in the model. Surprisingly the use of a static cut-off frequency of $f_H=0.515$ Hz, instead of the default value of 1 Hz, in SWAN using WAM-3 markedly improves both $\overline{Bias}$ and $\overline{NRMSE}$ for all bulk wave parameters. However, when the

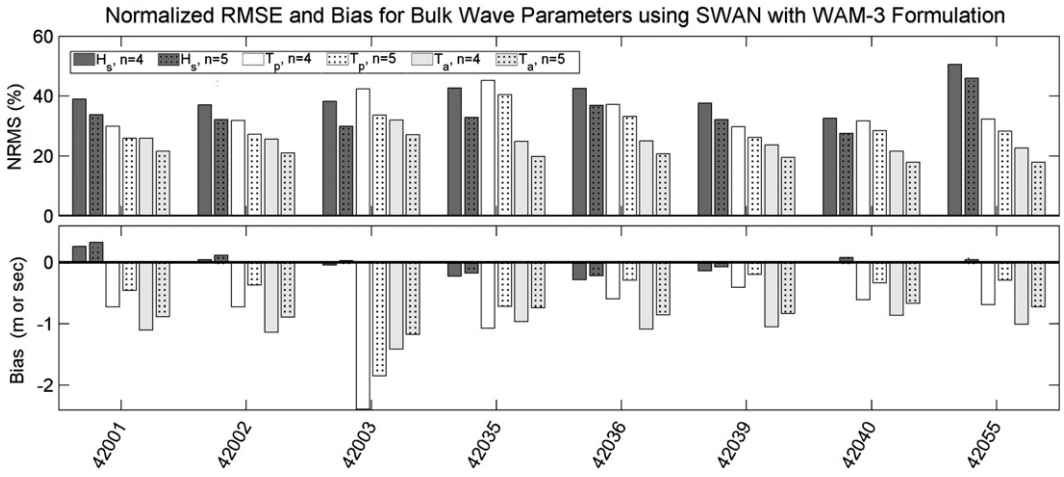

Fig. 5. The skill assessment of SWAN using WAM-3 formulation with $n=4$ and $n=5$, at all stations, for the first simulation time period, in terms of: a) Normalized root mean square error; b) Bias of bulk wave parameters. See Fig. 2 for station locations.

WAM-4 or Westhuysen formulations of SWAN were employed, little improvement was observed in term of $\overline{NRMSE}$. The more constrained tail ($f_H=0.515$ Hz) resulted in a lower bias of T_a, but in some cases slightly increased the bias of T_p when compared with corresponsing higher cut-off frequency case ($f_H=1$ Hz).

Among different formulations for SWAN, the WAM-3 was more sensitive to the exponent used in the frequency tail equation; and the use of $n=5$ resulted in better performance of the wave model than $n=4$. However, the WAM-4 formulation offered slight improvement only for T_a in terms of $\overline{NRMSE}$ using $n=5$ instead of $n=4$. The statistical indicators computed for all bulk wave parameters showed that the combnation of $f_H=0.515$ Hz and $n=5$ also results in the best agreement with measurements for both WAM-4 and Westhuysen formulations.

The performance of these formulations was also evaluated during an active Cold Front season at Gulf of Mexico; from November 2007 to May 2008. Since the dataset was long enough, the conventional definition of RMSE was used to evaluate the error statistics , which is defined as:

$$\mathrm{RMSE}=\sqrt{\frac{1}{N}\sum_{i=1}^{N}(X_{Oi}-X_{Mi})^2} \tag{5}$$

where $\overline{RMSE}$ is calculated based on the average value of RMSE for all available NDBC buoys (see Fig. 2). Better performance of SWAN using $n=5$, rather than $n=4$, in WAM-3 is apparent from Fig. 7. Moreover, regardless of the exponent used in the tail formulation, the use of $f_H=0.515$ Hz rather than $f_H=1$ Hz resulted in better $\overline{RMSE}$ and $\overline{Bias}$. The use of $n=5$ in tail form and $f_H=0.515$ Hz also enhanced the results of SWAN simulations using WAM-4 and Westhuysen formulations, but the improvements were not as conspicuous as in WAM-3.

3.3. Skill assessment of WAVEWATCH-III

The results from the WAVEWATCH-III simulations with a dynamic cut-off frequency of $f_H=0.515$ Hz and different formulations are provided in Fig. 8. Note that $n=4.5$ was used, instead of $n=5$, in WAVEWATCH-III with WAM-3 formulation, as suggested by Tolman (1992) to avoid noise in the high frequency end of the spectrum, due to dynamic time step algorithm used in the model. The use of $n=4.5$, rather than 4, improved the WAVEWATCH-III performance in terms of $\overline{\mathrm{Bias}}$ of mean wave period. The $\overline{\mathrm{Bias}}$ of T_p was also enhanced while the effects of using $n=4.5$ on H_s were insignificant.

The code of WAVEWATCH-III was modified such that it used the static cut-off frequency. The results from this modified model simulations are demonstrated in Fig. 8. Although the error statistics derived

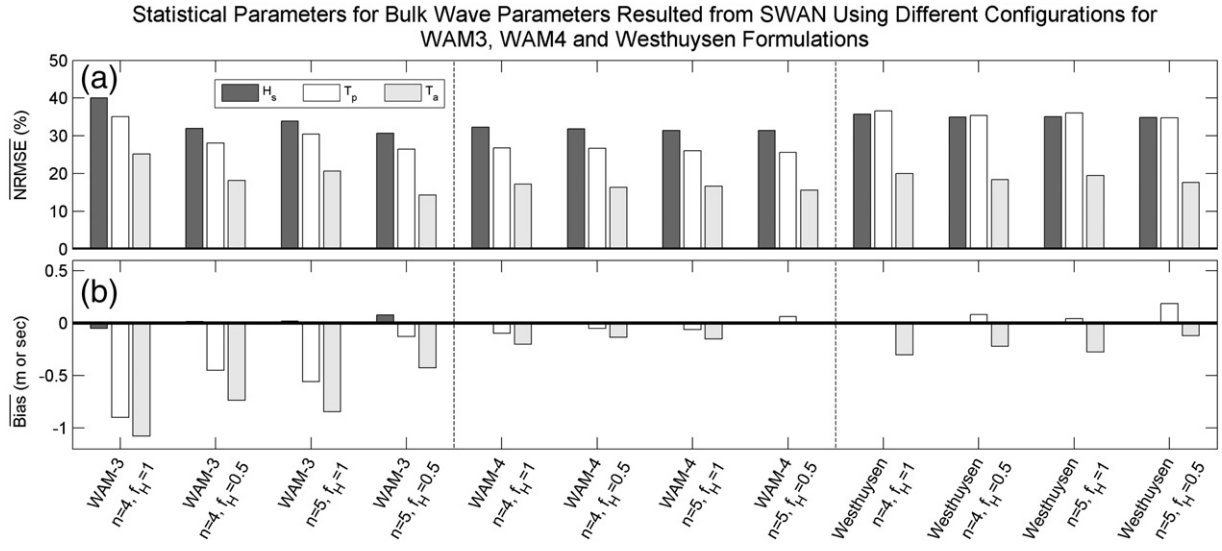

Fig. 6. The skill assessment of SWAN with different formulations and configurations based on all stations during the first simulation time period, in terms of: a) average of normalized root mean square error; b) averaged bias of bulk wave parameters.

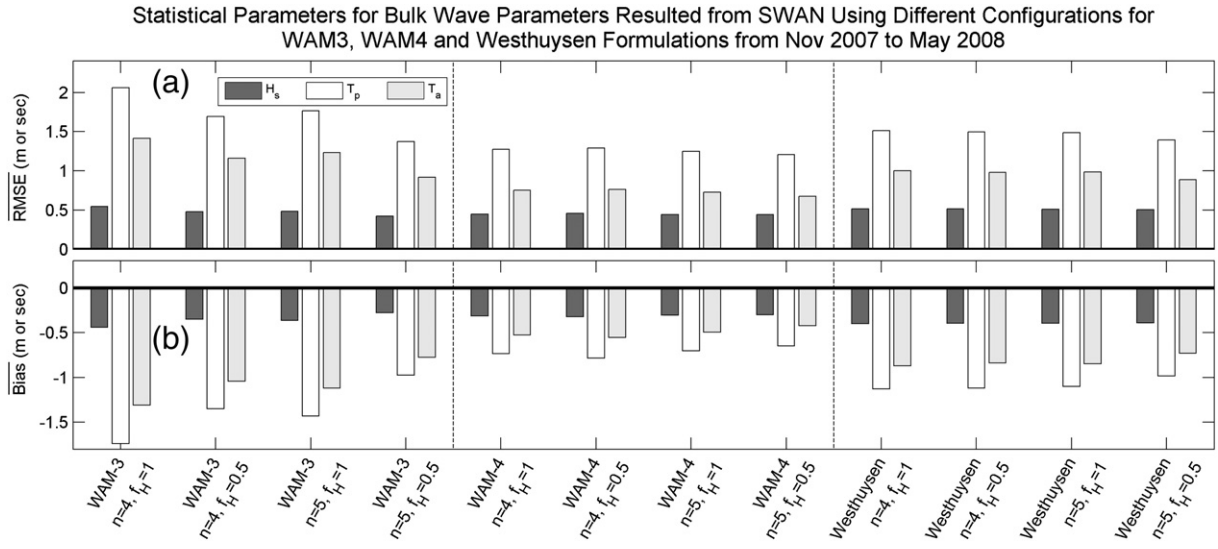

Fig. 7. The skill assessment of SWAN with different formulations and configurations, based on all stations with available data, during the second extended simulation time period (2007/2008 winter-spring Cold Front season) , in terms of: a) averaged root mean square error; b) averaged bias of bulk wave parameters.

from simulations using static cut-off frequency were close to corresponding simulations using dynamic cut-off frequency, the bias was slightly increased for all bulk wave parameters, especially during high energy events.

TC formulation showed different patterns compared with WAM formulation and worked better with $n=4$ than $n=5$; especially in terms of $\overline{\text{NRMSE}}$ of wave height. Also the $\overline{\text{Bias}}$ was smaller when $n=4$ for the frequency tail. Note that TC results were worse than WAM-3 for both $\overline{\text{Bias}}$ and $\overline{\text{NRMSE}}$ of H_s.

The better performance of WAM-3 formulation using $n=4.5$ in WAVEWATCH-III, rather than $n=4$, was also confirmed from the extended simulation of the 2007–2008 active Cold Front season. As shown in Fig. 9, both $\overline{\text{RMSE}}$ and $\overline{\text{Bias}}$ for T_a and T_p were in better agreement with observation when a higher value for n was used. Moreover, the statistics were close for both static and dynamic cut-off frequency of $f_H=0.515$ Hz. Unlike WAM formulations, the TC formulation worked better with $n=4$, as observed for the first simulation period.

3.4. Directional spread of energy

The directional distribution of energy from model also depends on the formulations used for whitecapping and wind input. To quantify the directional spread of energy, a non-dimensional directional width parameter can be defined, similar to the spectral width parameter (e.g., Massel (2007)):

$$\nu_D^2(f)=\frac{\hat{m}_0(f)\hat{m}_2(f)}{\hat{m}_1{}^2(f)}-1 \tag{6}$$

in which $\hat{m}_i(f)=\int_\theta \theta^i F(f,\theta)d\theta$. When the energy is concentrated in a directionally narrow band within a specific frequency bin, $\nu_D^2\to 0$ for that frequency bin; otherwise, ν_D^2 increases for directionally broad energy distribution.

The computed directional width parameter at the NDBC 42040 location using SWAN with WAM-3 and WAM-4 formulation, during

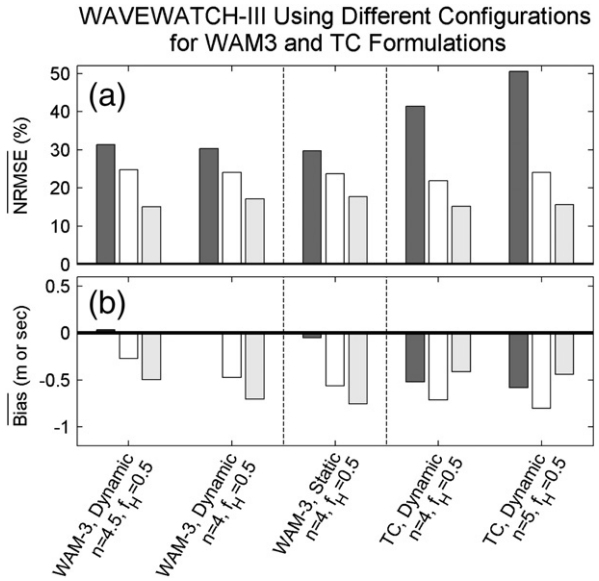

Fig. 8. The skill assessment of WAVEWATCH-III with different formulations and configurations based on all stations during the first simulation time period, in terms of: a) average of normalized root mean square error; b) averaged bias of bulk wave parameters.

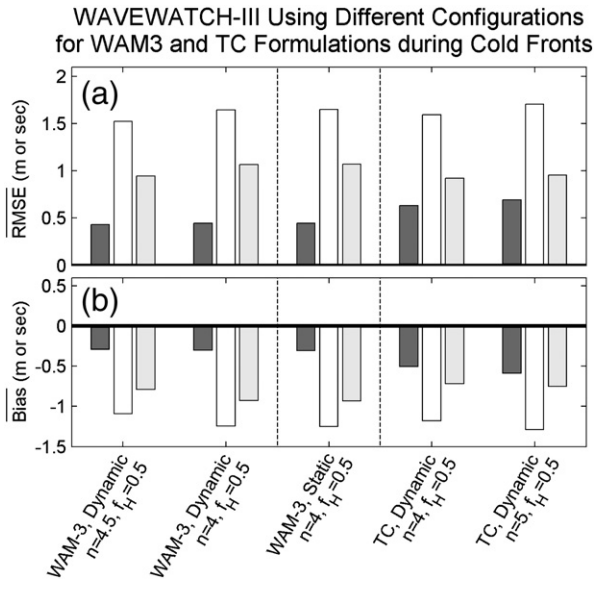

Fig. 9. The skill assessment of WAVEWATCH-III with different formulations and configurations based on all stations with available data during the second extended simulation time period (2007/2008 winter-spring Cold Front season), in terms of: a) averaged root mean square error; b) averaged bias of bulk wave parameters.

the hurricane period, is provided in Fig. 10. The data correspond to WAM-3 (left panels) and WAM-4 (right panels) formulations, at 5 discrete time steps during the passage of hurricanes Gustav and Ike through Gulf of Mexico: the start of intensification of H_s due to hurricane Gustav (panels a and f); peak H_s of hurricane Gustav from the simulations, which occurred 3 h after maximum H_s measured at NDBC 42040 (panels b and g); calm weather window between the two hurricane events (panels c and h); peak H_s of hurricane Ike, from the simulations, which was again with a 3 h time lag from the maximum H_s measured at the buoy (panels d and i); and relatively calm conditions after hurricane Ike (panels e and j). It is clear from all the different scenarios that WAM-3 led to a directionally broader tail as opposed to WAM-4. Moreover, WAM-3 was more sensitive to the change in the exponent of the frequency tail and the selection of f_H. The use of $n=5$ in WAM-3 resulted in a reduced energy in the tail, but the change of ν_D^2 at the spectral peak was negligible. However, the use of a lower f_H in WAM-3 broadened the distribution width at spectral peak during calm weather conditions (panel c) and the relaxation phase after the passage of a hurricane (panel e). Note that plots associated with peak waves of hurricanes were truncated before 1 Hz, because the peak energy was several orders of magnitude larger than the tail energy, and the truncated value of normalized energy level was zero at the high frequency tail in SWAN outputs.

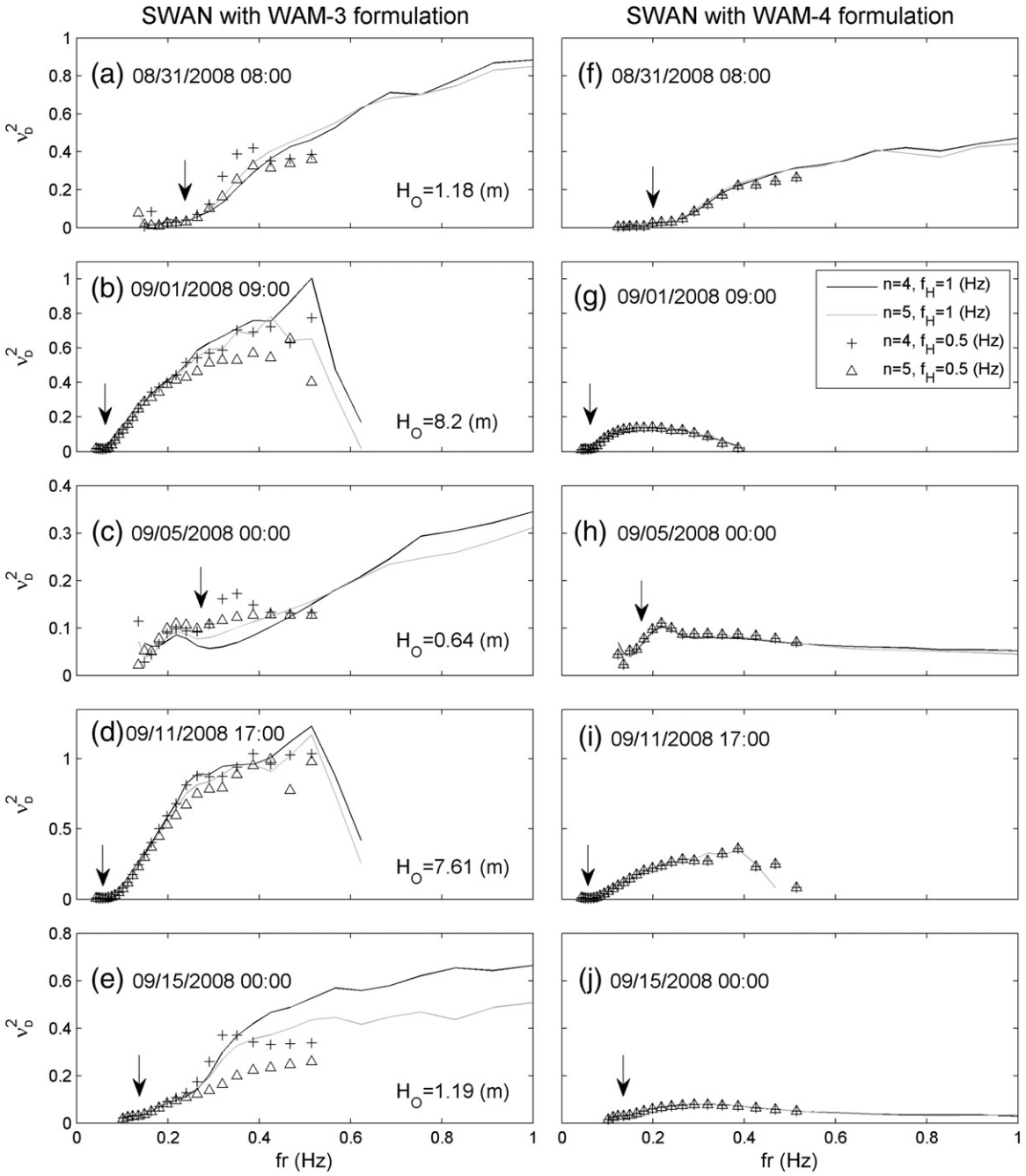

Fig. 10. The directional width of energy spread for different configurations of SWAN with WAM-3 (left panels) and WAM-4 (Right panels), at different time steps during the passage of hurricanes Gustav and Ike in 2008; at the location of NDBC buoy 42040. The location of the simulated peak frequency is shown by arrow. The wave heights measured by NDBC buoy 42040 at each time step are also provided in the left panels.

4. Discussion

4.1. Higher order dissipation term in WAM dissipation term

SWAN with the WAM-3 formulation systematically underestimated T_a. Fig. 4 shows that the energy levels at the rear face of the spectra were much more than the observed values. This is a well-known problem for SWAN using the WAM-3 formulation (Ris et al., 1999). The dissipation term of WAM-3 is a linear function of wave number normalized by mean wave number. Rogers et al. (2003) showed that the use of a quadratic dependence of dissipation on wavenumber can partially tackle the underestimation of period with two mechanisms: 1) more direct dissipation on higher wavenumbers (frequencies), 2) the mean wavenumber will also decrease when a quadratic dissipation term is used, which imposes more dissipation on the high frequency end of the spectrum. Although this approach was successful for field conditions in which wind speed and direction continuously varied, the use of this method for an idealized case and locally calibrated coefficients for the Gulf of Mexico, resulted in a spurious secondary peak in the front face of the spectrum (Siadatmousavi, 2011). The directional spectrum for an idealized wave growth condition, resulted from original Rogers et al. (2003) formulation is also different from WAM-3. For example, in case of non-stationary one dimensional simulation of wave growth under constant wind speed of 25 m/s, over a basin of 100 km long and 3000 m depth ($\Delta x = 1$ km, $\Delta t = 60$ s), the directional wave spectrum resulted from Rogers et al. (2003) formulation, for a fetch of 20 km, designates two secondary high energy peaks approximately 100° out of phase with wind. These two peaks concentrated close to 0.1 Hz and continued to grow slowly for few days, while the main peak (close to 0.16 Hz) which closely follows the wind direction, reached the equilibrium conditions after few hours. The results from the corresponding WAM-3 simulation did not show these low frequency features.

Banner and Young (1994) showed that the use of a higher order dissipation term in WAM-3 also results in a narrower directional spreading at the rear face of the spectrum and broader directional spreading near the spectral peak. As shown in Fig. 10, the suggestion of using lower cut-off frequency or a higher exponent value in the WAM-3 formulation of SWAN resulted in the same behavior at the rear face of the spectrum. However, a lower cut-off frequency also broadened the directional width close to the spectral peak. On the other hand, WAM-4 formulations were not sensitive to decrease in f_H. This feature also can be used to decrease the computational time needed to complete the simulation.

4.2. Cut-off frequency and tail slope

As shown in Figs. 6–**7**, the use of WAM-3 with the $n = 4$ exponent and constant high cut-off frequency, $f_H = 0.515$ Hz, outperformed the same configuration except with $f_H = 1$ Hz for the Gulf of Mexico. The use of smaller cut-off frequencies resulted in lower energy levels in the tail, and higher energy levels close to the spectral peak compared to the simulation with $f_H = 1$ Hz. Therefore exclusion of the frequency band 0.515–1 Hz from a prognostic frequency range for model applications could partially ameliorate the underestimation of T_a by WAM-3 formulation. The other two formulations of SWAN also showed better performance when $f_H = 0.515$ Hz was used as cut-off frequency rather than the default $f_H = 1$ Hz. This implies that none of the implemented formulations were capable of reproducing the physics of energy exchange and dissipation at the high frequency tail of spectrum. Therefore more advanced formulations are needed to extend the capabilities of phase averaged models for the accurate prediction of high frequency gravity waves.

The interaction of rear side of wave spectrum and frequencies close to the spectral peak was shown to be dependent on the formulation used for wind input, and for wave energy dissipation. The spectral evolution resulted from the WAM-4 or Westhuysen formulation was less sensitive than WAM-3, to variability in exponent of the high frequency tail; however, $n = 5$ still resulted in lower energy at the tail end and higher energy level close to the spectral peak, when compared with $n = 4$. The lower sensitivity of those formulations can be explained by higher energy dissipation imposed on the rear side of the spectrum. Therefore less energy is available for nonlinear interactions, which is a cubic function of the local spectral density function (Phillips, 1985).

The use of exponent $n = 5$ in the tail can be supported by previous studies, that affirmed the validity of theory of Phillips (1958) for the frequency spectrum at frequencies higher than $(2.5 - 3.5)f_p$; unless it is affected by the Doppler shifting effect. Therefore it raises a question why SWAN uses $n = 4$ in the high frequency end of the wave spectrum with most of its formulations? Note that the original value of the exponent in Eq. (2) was $n = 5$ in the original WAM-3 model (SWAMP Group, 1985) and WAM-4 model (Komen et al., 1994). Although not mentioned in the SWAN manual, the value of $n = 4$ is more suitable for application in shallow water, in which the exponent is smaller (as discussed in Section 1.1). Moreover, SWAN was originally designed for coastal area applications, in which the fetch is limited for most wind directions. There are several parametric wave growth curves for deep water in which peak frequency, f_p, is proportional to X^m, in which X is fetch length and the coefficient m varies from -0.23 to -0.33 (Donelan et al., 1985; Hasselmann et al., 1973; Kahma, 1981). Similar inverse dependency exists for shallow water wave dynamics (e.g., see Fig. **7**.17 in Young (1999)). Therefore in fetch limited area, the peak frequency is higher, and therefore equilibrium range of spectrum (less than $3f_p$) is more extended. As discussed in Section 1.1, $n = 4$ is in better agreement with the observed data in equilibrium range. On the other hand, the original value of $n = 5$ in WAM-4 was not changed. One explanation can be the fact that the calculation of wind induced shear in WAM-4 formulation was reported to be sensitive to the value of n (Komen et al., 1994).

4.3. Dynamic and static cut-off frequency

The uses of WAM-3 formulation with similar configurations but with a constant cut-off frequency of $f_H = 0.515$ Hz, slightly worsen the performance of the WAVEWATCH-III. It is suggested that the use of a dynamic high cut-off frequency not only optimizes the model calculations, but also improves its performance on oceanic scales, such as for the Gulf of Mexico. According to the definition of dynamic cut-off frequency given in Section 2.2, it differs from the static one only when 2.5 times of the mean frequency is less than the user-defined value for cut-off frequency. Since the peak frequency (and therefore mean frequency for usual mono-modal spectrums) is inversely related to wind speed (e.g., parametric formulation of Hasselmann et al. (1973)), the mean wave frequency decreases with increase in wave height for wind seas. Therefore the difference between static and dynamic cut-off frequency becomes more important for energetic events. In order to bolster this finding, the following analysis was pursued. The difference between H_s and T_a simulated from WAVEWATCH-III, at all NDBC stations shown in Fig. 2, and using a static and dynamic cut-off frequency of $f_H = 0.515$ Hz, are normalized with simulated bulk wave parameters from model with dynamic cut-off frequency ($H_{s,Dyn}$ and $T_{p,Dyn}$ respectively). The mean values for the change in normalized H_s and T_a, from all *in situ* observations, were plotted in Fig. 11 against $H_{s,Dyn}$, with a bin size of 0.2 m for $H_{s,Dyn}$. During energetic events, the static cut-off frequency is higher than equilibrium range of spectrum, and nonlinear interaction pumps part of energy beyond equilibrium range. Therefore the wave spectrum evolves at slower pace during high energy events, when constant cut-off is employed in the model. This is consistent

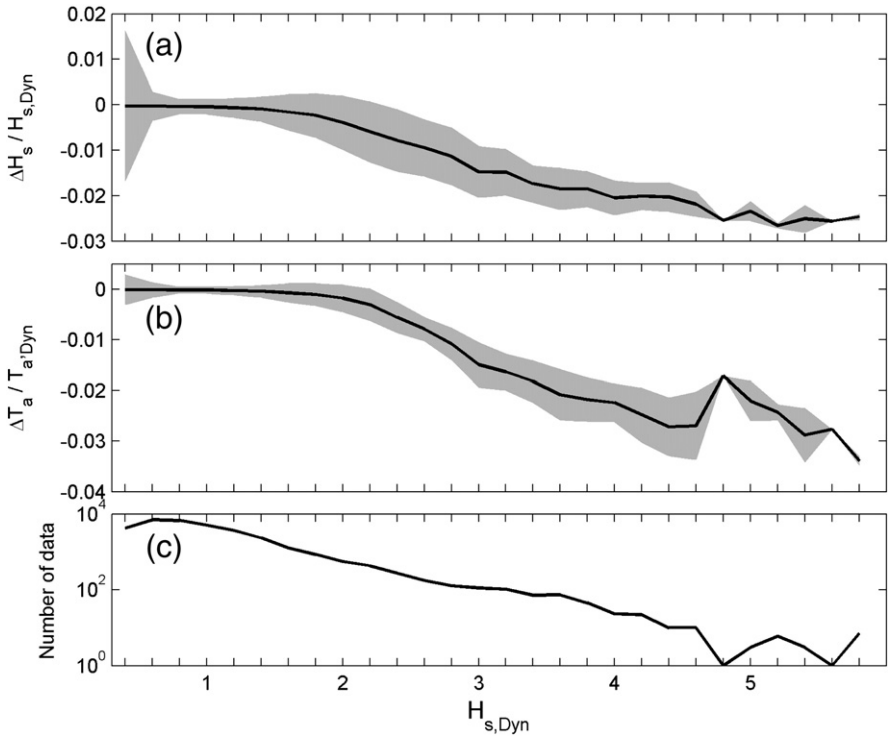

Fig. 11. a) The difference between simulated wave height from WAM-3 formulation with dynamic and static cut-off frequency ($H_{s,static}$–$H_{s,dynamic}$) normalized by $H_{s,dynamic}$ versus $H_{s,dynamic}$; b) the normalized difference of T_a versus $H_{s,dynamic}$; c) the number of data points occurred within each bin (bin size was equal to 0.2 m). The shadings show one standard deviation higher and lower than mean value at each bin.

with Banner and Young (1994) argument on excessive energy transfer to high frequency tail by WAM-3 formulation and its slower growth rate when unconstrained tail was used. As waves become more energetic, the mean frequency decreases and the gap between cut-off frequency and end of equilibrium range increases; therefore the difference between two model configurations increases.

It is important to note that the high cut-off frequency is treated as static value in SWAN, given the fact that this model was originally formulated for shallow water simulations, in which complex wave fields make it difficult to delineate one main active wave system with smooth and a stable dynamic cut-off frequency (Booij et al., 1999). Therefore for oceanic scales, it is recommended to use dynamic cut-off frequency to decrease the computational cost as well as to facilitate more realistic energy transfer to high frequency tail of the spectrum.

4.4. Performance of TC formulation

Figs. 8–9 show that the use of $n=4$, rather than $n=5$, in TC formulation of WAVEWATCH-III resulted in a better estimation of the bulk wave parameters (especially H_s). The disparity between TC formulation and WAM-3 in WAVEWATCH-III is caused by severe underestimation of energy in low frequencies. Ardhuin et al. (2010) also reported negative bias and low performance of TC formulation in Lake Michigan (see Table 2 in their paper). Based on the good performance of TC formulation in open oceans, they concluded that there is a scale-dependency in TC equations. It was mentioned in Section 1 that the dissipation term of TC composed of two terms: a low frequency constituent and one dedicated formulation for the contribution of high frequency waves. The difference between modeled and

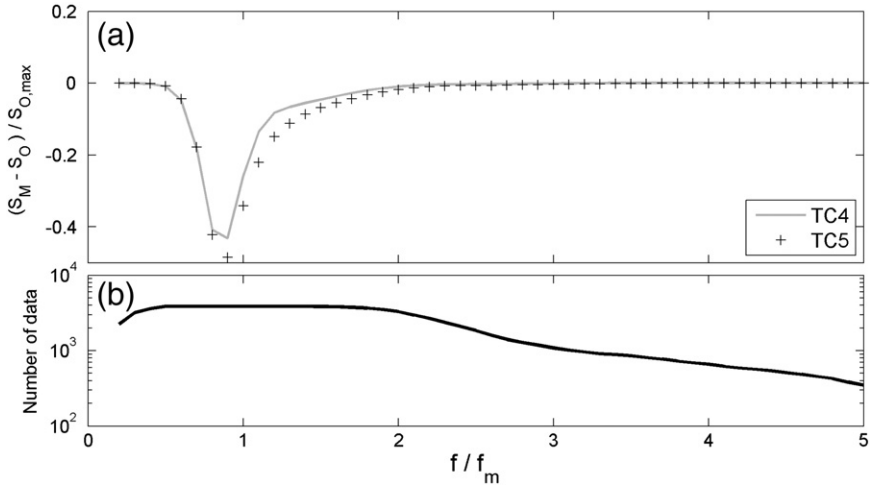

Fig. 12. a) The average of normalized spectrum bias using TC formulation for the second extended simulation time period (2007/2008 winter–spring Cold Front season); b) the number of data points occurred within each bin (bin size was set to 0.1).

observed wave spectrum was normalized with spectral peak of the measured spectra for 2007/2008 winter-spring Cold Front season, and the mean value was plotted versus normalized frequency in Fig. 12. As highlighted, the underestimation mainly occurred close to the mean frequency; therefore low frequency constituent of TC dissipation term needs to be adjusted before modifying the tail parameters, which could have secondary effects on the results of simulation.

5. Conclusions and summary

Parameter evaluation of SWAN and WAVEWATCH-III models for simulating calm and severe weather conditions at Gulf of Mexico yielded the following conclusions:

1) The WAM-3 formulation was very sensitive to the assumed high cut-off frequency and assumed power law for the diagnostic frequency tail.
2) The numerical simulations confirmed better performance of the model with $n=5$ in the diagnostic tail in terms of bias and root mean square error of bulk wave parameters. Hence, in oceanic scales, the use of $n=5$, rather than the default value of $n=4$, is recommended for SWAN.
3) The use of WAM-3 formulation for wind input and whitecapping dissipation in wave model resulted in too much energy in the frequencies beyond the equilibrium range of spectrum which was the main reason for a well-known underestimation of average wave period. Therefore, in oceanic scale wave modeling, the use of the more limited range ($f_H=0.5$ Hz rather than $f_H=1$ Hz) for prognostic part of the wave spectrum is suggested for SWAN when WAM-3 formulation is employed.
4) The use of WAM-3 in WAVEWATCH-III with a dynamic high cut-off frequency slightly outperformed the corresponding simulation using constant high cut-off frequency, when implemented for the Gulf of Mexico. This indicates that, to use SWAN in the oceanic scales, the implementation of dynamic cut-off frequency not only decreases the computational cost but also enhances the simulation results.
5) The WAM-4 and Westhuysen formulations in SWAN for simulations conducted in Gulf of Mexico were least affected by the exponent used for the exponential tail form or the assumed high cut-off frequency. This feature can be used to optimize the time needed to perform a simulation by using a lower f_H, and compensate for more calculations needed for a wind energy term of WAM-4; or whitecapping term of Westhuysen formulation when compared with corresponding formulation of WAM-3. The higher dissipation imposed on the rear side of the spectrum in these formulations resulted in a reduced energy level in the frequency tail, even when prognostic region of the wave spectrum is extended to 1 Hz. The low energy content in the high frequency end of the spectrum indicates less energy exchange by nonlinear wave interaction; which could explain narrower energy distribution in the rear side of the WAM-4 simulated spectrum, when compared with WAM-3 results.
6) The non-WAM formulation of WAVEWATCH-III, proposed by Tolman and Chalikov (1996) package with its default values for its free parameters resulted in considerably too strong energy dissipation for the Gulf of Mexico. A new calibration process is needed to remedy the underestimation of wave height simulated by this formulation.

Acknowledgements

The authors wish to thank Dr. Marcel Zijlema (Delft University of Technology) for sharing the source code for parallel unstructured SWAN before its official release. Jonathan R. Shewchuk (UC-Berkeley) developed the Triangle grid generation tool used in this study. We are grateful to Professor Alexander Babanin and another anonymous reviewer for their invaluable comments and suggestions on a previous draft. The continuing support from WAVCIS lab colleagues for processing the data is gratefully acknowledged.

References

Alves, J.H.G.M., Greensladeb, D.J.M., Banner, M.L., 2002. Impact of a saturation-dependent dissipation source function on operational hindcasts of wind-waves in the Australian region. Journal of Atmospheric & Ocean Science 8 (4), 239–267.
Anctil, F., Donelan, M.A., Forristall, G.Z., Steele, K.E., Ouellet, Y., 1993. Deep-water field-evaluation of the ndbc-swade 3-m discus directional buoy. Journal of Atmospheric and Oceanic Technology 10 (1), 97–112.
Ardhuin, F., et al., 2007. Swell and slanting-fetch effects on wind wave growth. Journal of Physical Oceanography 37 (4), 908–931.
Ardhuin, F., et al., 2010. Semiempirical dissipation source functions for ocean waves. Part i: Definition, calibration, and validation. Journal of Physical Oceanography 40 (9), 1917–1941.
Babanin, A.V., Tsagareli, K.N., Young, I.R., Walker, D.J., 2010. Numerical investigation of spectral evolution of wind waves. Part ii: dissipation term and evolution tests. Journal of Physical Oceanography 40 (4), 667–683.
Banner, M.L., 1990. Equilibrium spectra of wind-waves. Journal of Physical Oceanography 20 (7), 966–984.
Banner, M.L., 1991. On the directional behavior of the equilibrium wave number spectrum: implications for the equilibrium frequency spectrum. In: Beal, R.C. (Ed.), Directional Ocean Wave Spectra. Johns Hopkins University Press, Baltimore, pp. 39–45.
Banner, M.L., Young, I.R., 1994. Modeling spectral dissipation in the evolution of wind-waves. 1. Assessment of existing model performance. Journal of Physical Oceanography 24 (7), 1550–1571.
Banner, M.L., Jones, I.S.F., Trinder, J.C., 1989. Wavenumber spectra of short gravity-waves. Journal of Fluid Mechanics 198, 321–344.
Battjes, J.A., Janssen, J.P.F.M., 1978. Energy loss and set-up due to breaking of random waves. 16th International Conference on Coastal Engineering, ASCE, pp. 569–587.
Berg, R., 2008. Tropical Cyclone Report Hurricane Ike. National Hurricane Centre, National Oceanographic and Atmospheric Administration, Miami, Florida.
Beven, J.L., Kimberlain, T.B., 2008. Tropical Cyclone Report Hurricane Gustav. National Hurricane Centre, National Oceanographic and Atmospheric Administration, Miami, Florida.
Bilgili, A., Smith, K.W., Lynch, D.R., 2006. Battri: a two-dimensional bathymetry-based unstructured triangular grid generator for finite element circulation modeling. Computers & Geosciences-Uk 32 (5), 632–642.
Booij, N., Ris, R.C., Holthuijsen, L.H., 1999. A third-generation wave model for coastal regions — 1. Model description and validation. Journal of Geophysical Research, Oceans 104 (C4), 7649–7666.
Cavaleri, L., Rizzoli, P.M., 1981. Wind wave prediction in shallow-water — theory and applications. Journal of Geophysical Research, Oceans Atmospheres 86 (Nc11), 961–973.
Cavaleri, L., et al., 2007. Wave modelling — the state of the art. Progress in Oceanography 75 (4), 603–674.
Chalikov, D., 1995. The parameterization of the wave boundary-layer. Journal of Physical Oceanography 25 (6), 1333–1349.
Chalikov, D.V., Belevich, M.Y., 1993. One-dimensional theory of the wave boundary-layer. Boundary-Layer Meteorology 63 (1–2), 65–96.
Donelan, M.A., Hamilton, J., Hui, W.H., 1985. Directional spectra of wind-generated waves. Philosophical Transactions of the Royal Society A 315 (1534), 509–562.
Ewans, K.C., Kibblewhite, A.C., 1990. An examination of fetch-limited wave growth off the west-coast of new-zealand by a comparison with the jonswap results. Journal of Physical Oceanography 20 (9), 1278–1296.
Forristall, G.Z., 1981. Measurements of a saturated range in ocean wave spectra. Journal of Geophysical Research, Oceans Atmospheres 86 (Nc9), 8075–8084.
Hansen, C., Katsaros, K.B., Kitaigorodskii, S.A., Larsen, S.E., 1990. The dissipation range of wind-wave spectra observed on a lake. Journal of Physical Oceanography 20 (9), 1264–1277.
Hasselmann, K., 1963. On the non-linear energy transfer in a gravity-wave spectrum. 3. Evaluation of the energy flux and swell-sea interaction for a neumann spectrum. Journal of Fluid Mechanics 15 (3), 385–398.
Hasselmann, K., 1974. On the spectral dissipation of ocean waves due to white capping. Boundary-Layer Meteorology 6 (1–2), 107–127.
Hasselmann, K., 1988. The wam model — a 3rd generation ocean wave prediction model. Journal of Physical Oceanography 18 (12), 1775–1810.
Hasselmann, S., Hasselmann, K., 1985. Computations and parameterizations of the nonlinear energy-transfer in a gravity-wave spectrum. 1. A new method for efficient computations of the exact nonlinear transfer integral. Journal of Physical Oceanography 15 (11), 1369–1377.
Hasselmann, K., et al., 1973. Measurements of wind-wave growth and swell decay during the joint north sea wave project (JONSWAP). Deutsche Hydrographische Zeitschrift A8 No 12.
Hasselmann, S., Hasselmann, K., Allender, J.H., Barnett, T.P., 1985. Computations and parameterizations of the nonlinear energy-transfer in a gravity-wave spectrum. 2. Parameterizations of the nonlinear energy-transfer for application in wave models. Journal of Physical Oceanography 15 (11), 1378–1391.
Hwang, P.A., Atakturk, S., Sletten, M.A., Trizna, D.B., 1996. A study of the wavenumber spectra of short water waves in the ocean. Journal of Physical Oceanography 26 (7), 1266–1285.

Janssen, P.A.E.M., 1991. Quasi-linear theory of wind-wave generation applied to wave forecasting. Journal of Physical Oceanography 21 (11), 1631–1642.
Janssen, P.A.E.M., 2004. The Interaction of Ocean Waves and Wind. Cambridge University Press. 300 pp.
Janssen, P.A.E.M., 2008. Progress in ocean wave forecasting. Journal of Computational Physics 227 (7), 3572–3594.
Janssen, P.A.E.M., et al., 1994. Simple tests. In: Komen, G.J., et al. (Ed.), Dynamics and Modelling of Ocean Waves. Cambridge University Press, p. 556.
Kahma, K.K., 1981. A study of the growth of the wave spectrum with fetch. Journal of Physical Oceanography 11 (11), 1503–1515.
Kitaigordskii, S.A., Krasitskii, V.P., Zaslavskii, M.M., 1975. Phillips theory of equilibrium range in spectra of wind-generated gravity-waves. Journal of Physical Oceanography 5 (3), 410–420.
Kitaigorodskii, S.A., 1983. On the theory of the equilibrium range in the spectrum of wind-generated gravity-waves. Journal of Physical Oceanography 13 (5), 816–827.
Komen, G.J., Hasselmann, S., Hasselmann, K., 1984. On the existence of a fully-developed wind-sea spectrum. Journal of Physical Oceanography 14 (8), 1271–1285.
Komen, G.J., et al., 1994. Dynamics and Modelling of Ocean Waves. Cambridge University Press, Cambridge. 532 pp.
Leykin, I.A., Rozenberg, A.D., 1984. Sea-tower measurements of wind-wave spectra in the Caspian Sea. Journal of Physical Oceanography 14 (1), 168–176.
Li, C.W., Mao, M., 1992. Spectral modeling of typhoon-generated waves in shallow waters. Journal of Hydraulic Research 30 (5), 611–622.
Liu, P.C., 1989. On the slope of the equilibrium range in the frequency-spectrum of wind-waves. Journal of Geophysical Research, Oceans 94 (C4), 5017–5023.
Massel, S.R., 2007. Ocean waves breaking and marine aerosol fluxes. Atmospheric and Oceanographic Sciences Library. Springer, New York. 328 pp.
Mitsuyasu, H., 1977. Measurement of high-frequency spectrum of ocean surface-waves. Journal of Physical Oceanography 7 (6), 882–891.
Mitsuyasu, H., et al., 1980. Observation of the power spectrum of ocean waves using a cloverleaf buoy. Journal of Physical Oceanography 10 (2), 286–296.
Phillips, O.M., 1958. The equilibrium range in the spectrum of wind-generated waves. Journal of Fluid Mechanics 4 (4), 426–433.
Phillips, O.M., 1985. Spectral and statistical properties of the equilibrium range in wind-generated gravity-waves. Journal of Fluid Mechanics 156, 505–531 (Jul).
Pierson, W.J., Moskowitz, L., 1964. Proposed spectral form for fully developed wind seas based on similarity theory of S A Kitaigorodskii. Journal of Geophysical Research 69 (24), 5181–5190.
Resio, D., Perrie, W., 1991. A numerical study of nonlinear energy fluxes due to wave–wave interactions. 1. Methodology and basic results. Journal of Fluid Mechanics 223, 603–629.
Ris, R.C., Holthuijsen, L.H., Booij, N., 1999. A third-generation wave model for coastal regions — 2. Verification. Journal of Geophysical Research, Oceans C4, 7667–7681.
Rodriguez, G., Soares, C.G., 1999. Uncertainty in the estimation of the slope of the high frequency tail of wave spectra. Applied Ocean research 21 (4), 207–213.
Rodriguez, G., Soares, C.G., Ocampo-Torres, F.J., 1999. Experimental evidence of the transition between power law models in the high frequency range of the gravity wave spectrum. Coastal Engineering 38 (4), 249–259.
Rogers, W.E., Hwang, P.A., Wang, D.W., 2003. Investigation of wave growth and decay in the swan model: three regional-scale applications. Journal of Physical Oceanography 33 (2), 366–389.
Sheremet, A., Stone, G.W., 2003. Observations of nearshore wave dissipation over muddy sea beds. Journal of Geophysical Research, Oceans 108 (C11).
Siadatmousavi, S.M., 2011. Valuation of two wam white capping parameterizations using parallel unstructured swan with application to the northern gulf of mexico, USA. Applied Ocean Research 33, 23–30.
Siadatmousavi, S.M., Jose, F., Stone, G.W., 2009. Simulating hurricane Gustav and ike wave fields along the louisiana innershelf: implementation of an unstructured third-generation wave model, swan., Oceans'09, Biloxi, Mississippi, pp. 1–12.
Snyder, R.L., Dobson, F.W., Elliott, J.A., Long, R.B., 1981. Array measurements of atmospheric-pressure fluctuations above surface gravity-waves. Journal of Fluid Mechanics 102, 1–59 (Jan).
Swail, V.R., Cox, A.T., 2000. On the use of ncep-ncar reanalysis surface marine wind fields for a long-term north atlantic wave hindcast. Journal of Atmospheric and Oceanic Technology 17 (4), 532–545.
SWAMP Group, 1985. Ocean Wave Modeling. Plenum Press, New York and London.
SWAN team, 2010. Swan Cycle iii version 40.81, Scientific and Technical Documentation.
Thornton, E.B., 1977. Re-derivation of saturation range in frequency-spectrum of wind-generated gravity-waves. Journal of Physical Oceanography 7 (1), 137–140.
Toba, Y., 1973. Local balance in the air-sea boundary processes, iii. On the spectrum of wind waves. Journal of Oceanographical Society of Japan 29, 209–220.
Tolman, H.L., 1992. Effects of numerics on the physics in a 3rd-generation wind-wave model. Journal of Physical Oceanography 22 (10), 1095–1111.
Tolman, H.L., 2009. User Manual and System Documentation of Wavewatch iii™ version 3.14, NOAA/NWS/NCEP/MMAB Technical Note 276.
Tolman, H.L., Chalikov, D., 1996. Source terms in a third-generation wind wave model. Journal of Physical Oceanography 26 (11), 2497–2518.
van der Westhuysen, A.J., Zijlema, M., Battjes, J.A., 2007. Nonlinear saturation-based white capping dissipation in swan for deep and shallow water. Coastal Engineering 54 (2), 151–170.
van Vledder, G.P., 2006. The wrt method for the computation of non-linear four-wave interactions in discrete spectral wave models. Coastal Engineering 53 (2–3), 223–242.
van Vledder, G.P., Bottema, M., 2003. Improved modelling of nonlinear four-wave interactions in shallow water. 28th International Conference on Coastal Engineering. ASCE, Cardif, Wales, pp. 459–471.
Westerink, J.J., Luettich, R.A., Baptista, A.M., Scheffner, N.W., Farrar, P., 1992. Tide and storm-surge predictions using finite-element model. Journal of Hydraulic Engineering ASCE 118 (10), 1373–1390.
Yan, L., 1987. An Improved Wind Input Source Term for Third Generation Ocean Wave Modelling. Royal Dutch Metrology Institute, pp. 87–88.
Young, I.R., 1999. Wind generated ocean waves. Elsevier Ocean Engineering Series. Elsevier. 306 pp.
Young, I.R., Babanin, A.V., 2006. Spectral distribution of energy dissipation of wind-generated waves due to dominant wave breaking. Journal of Physical Oceanography 36 (3), 376–394.
Young, I.R., Vanvledder, G.P., 1993. A review of the central role of nonlinear-interactions in wind wave evolution. Philosophical Transactions of the Royal Society A 342 (1666), 505–524.
Young, I.R., Verhagen, L.A., 1996. The growth of fetch limited waves in water of finite depth .2. Spectral evolution. Coastal Engineering 29 (1–2), 79–99.
Zubier, K., Panchang, V., Demirbilek, Z., 2003. Simulation of waves at duck (north carolina) using two numerical models. Coastal Engineering Journal 45 (3), 439–469.